

Study of Aggregation of Gold Nanoparticles in Chitosan

**Galo Cárdenas-Triviño & Christian
Cruzat-Contreras**

Journal of Cluster Science
Including Nanoclusters and
Nanoparticles

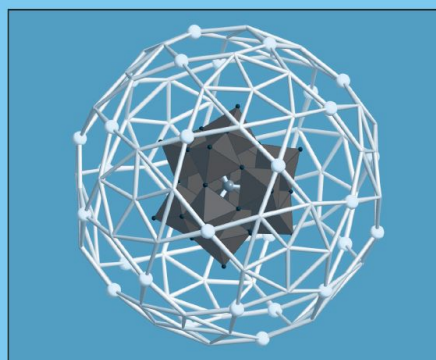
ISSN 1040-7278

J Clust Sci
DOI 10.1007/s10876-018-1419-x

Volume 24, Number 3

**ONLINE
FIRST**

JOURNAL OF CLUSTER SCIENCE
INCLUDING NANOCLUSTERS
AND NANOPARTICLES



 Springer

Available
online
www.springerlink.com

 Springer

Your article is protected by copyright and all rights are held exclusively by Springer Science+Business Media, LLC, part of Springer Nature. This e-offprint is for personal use only and shall not be self-archived in electronic repositories. If you wish to self-archive your article, please use the accepted manuscript version for posting on your own website. You may further deposit the accepted manuscript version in any repository, provided it is only made publicly available 12 months after official publication or later and provided acknowledgement is given to the original source of publication and a link is inserted to the published article on Springer's website. The link must be accompanied by the following text: "The final publication is available at link.springer.com".



Study of Aggregation of Gold Nanoparticles in Chitosan

Galo Cárdenas-Triviño¹ · Christian Cruzat-Contreras²

Received: 25 May 2018

© Springer Science+Business Media, LLC, part of Springer Nature 2018

Abstract

In this work it is reported the synthesis of gold nanoparticles supported in situ in chitosan by solvated metal atom dispersion technique in order to study the inclusion of Au nanoparticles in the biopolymer matrix. To study their aggregation along time and compare with the synthesis of Au/2-propanol colloid by chemical liquid deposition technique. Studies of Au nanoparticles aggregation along time, supported nanoparticles and colloidal nanoparticles morphology were also carried out. The characterization of Au nanoparticles was performed by transmission electron microscopy, field-emission and scanning electron microscopy, infrared spectroscopy, X-ray diffraction, light scattering and ultraviolet-visible spectroscopy. Metal colloid showed fractal agglomeration type and delay time after the synthesis, the agglomeration size increased to flocculate. Au nanoparticles supported in chitosan showed the same shape as colloids and fractal aggregation was mostly distributed on the matrix.

Keywords Nanostructures · Polymer · Transmission electron microscopy (TEM) · Colloid agglomeration · Supported nanoparticles

Introduction

The organization of nanoparticles in two- or three-dimensions (nanocrystals, films or quantum dots) as well as the understanding and characterization of these materials have become in a very important subject because of the different properties [1] shown by these composites, in comparison to individual particles [2]. Solvated metal atom dispersion (SMAD) technique involves the vaporization of the metal in a high vacuum reactor and the co-deposition of metallic vapor on the freeze reactor walls at liquid nitrogen temperature [3]. The metal atoms in the reaction are stabilized by an organic solvent, forming a solvation sphere, before they reach the frozen reactor walls. After the reaction, nanoparticles are warming to room temperature to form

metal colloids, in this step, the nanoparticles aggregation is produced in different shapes (spherical, clusters, fractals, etc.), depending on the metal concentration; metal type, organic solvent and delay time to stabilize the colloidal nanoparticles [4]. The SMAD technique has the advantage of not producing salts by reduction and stabilization of metal nanoparticles in a polymer matrix at the time of synthesis, avoiding metal agglomeration and oxidation of metal nanoparticles. There is a great interest in these compounds because they can be used in medicine as antibacterial coatings, because of biocidal action provided by the Au nanoparticles (AuNps). Indeed, several selective homogeneous catalysts from nanoparticles have been reported and the only feature is the ability of the polymer chain to protect and stabilize the metal particles from oxidation, allowing the penetration of the reagents for the desired catalytic reactions [5].

✉ Galo Cárdenas-Triviño
gcardenas@ubiobio.cl

Christian Cruzat-Contreras
christiancruzat@gmail.com

¹ Facultad de Ingeniería, DIMAD, Centro de Biomateriales y Nanotecnología, Universidad del Bío-Bío, Av. Collao 1202, Concepción, Chile

² CEDIA-Proyectos, Universidad de Cuenca, Cuenca, Ecuador

Methodology

Materials

Chitosan (CS), with a molecular weight of 4.8×10^5 g/mol, was purchased from Quitoquímica Co.

(Coronel, VIII Region, Chile). The degree of deacetylation was 98%, which was determined by infrared spectroscopy. Metallic Au was obtained from Aldrich. 2-propanol was purchased from Fisher (Pittsburgh, PA, USA). All the glassware was cleaned by using aqua regia solution (HCl/HNO₃ 3:1 v/v) and subsequently rinsed with copious amounts of 2-propanol reactive grade.

Synthesis of Au/2-Propanol Colloid

Au/2-propanol colloid (abbreviated as coll. from here on) was prepared by chemical liquid deposition (CLD) method [6], which involved vapor deposition of metallic Au in organic vapor media. The metallic atom reaction was carried out in a glass reactor. A W-Al₂O₃ crucible loaded with Au was assembled in the metal atom reactor and the whole system was evacuated. A glass device with the organic solvent (2-propanol), dried with molecular sieves and further degasified three times by standard freeze–thaw procedure [7], was attached to the neck of the reactor. The whole system was immersed in liquid nitrogen (77 K) and evacuated to reach the vacuum at 10⁻⁵ bar. The W-Al₂O₃ crucible was heated at 40 A until Au boiling point. In the reaction, the metallic Au and the solvent (2-propanol) were co deposited over half an hour. The frozen matrix, obtained on the reactor walls, was allowed to warm slowly for 1 h. After this time, the reactor was filled with extra pure nitrogen gas. After 30 min under nitrogen flow, Au colloidal dispersion in 2-propanol was obtained. In a typical reaction, 0.2 mmol of Au was evaporated with 100 mL of 2-propanol (dried and degassed) to obtain the Au/2-propanol coll.

Preparation of Au/2-Propanol Coll. CS Composite

In the same way, the Au colloid was prepared initially with the high molecular weight CS and introduced into the reactor. The reactor was kept under vacuum until reaching 5–10 mm of Hg, previously the chitosan powder (2.0 g) has been introduced with a magnetic stirrer inside the metal atom reactor.

Electron Microscopy Studies

Particles size for colloidal dispersions were calculated by a histogram analysis of the micrographs obtained with a TEM (JEOL-JEM 1200EXII) with 4 Å resolution. A drop of each Au coll. was placed on a dry copper grid (150 mesh), previously coated with carbon, in an inert atmosphere. The particle size distribution diameter were randomly measured and data obtained was represented by a histogram and fitted with normal curve reported by Fig. 1. Field-emission scanning electron microscopy (FESEM) analysis of CS-Au NPs. was carried out in a JEOL-JSM

6301F. FESEM was used to examine representative powder surfaces and samples that were not coated with gold.

UV Spectroscopy

UV absorption spectra of colloidal particles (0.01% v/v) were collected at 25 °C using a UV spectrophotometer (Shimadzu Corp, Kyoto Japan). Absorption spectra were recorded from 200 to 1100 nm, using quartz cells. 2-propanol was used as blank for each colloid and examined at different times. The kinetics of nanoparticles agglomeration was studied at room temperature.

FT-IR Spectroscopy

Infrared spectra were recorded from 100 to 4000 cm⁻¹ on a Nicolet Nexus spectrometer at room temperature (Nicolet Instrument Co., USA). Solids were obtained by solvent evaporation in inert atmosphere and pressed into pellets with solid KBr. Spectra were recorded at 4 cm⁻¹ of resolution and 64 scans were accumulated.

Thermogravimetric (TGA) Analysis

TGA experiments were carried out using a Thermogravimeter Analyzer Perkin Elmer TGA 7. All experiments were carried out under nitrogen atmosphere. All specimens were weighted in the range of 3–5 mg and heated at rate of 10 °C/min until 550 °C.

Light Scattering (LS) Analysis

The light scattering measurements were made with LS-instrument Brookhaven Instruments Corp. 90 plus/BI-MAS with an incidence angle of 90° by colloid and analysis data were carried out the particle size were carried out in Software © Ver 3.74. The samples were not filtered and they were diluted in the same solvent.

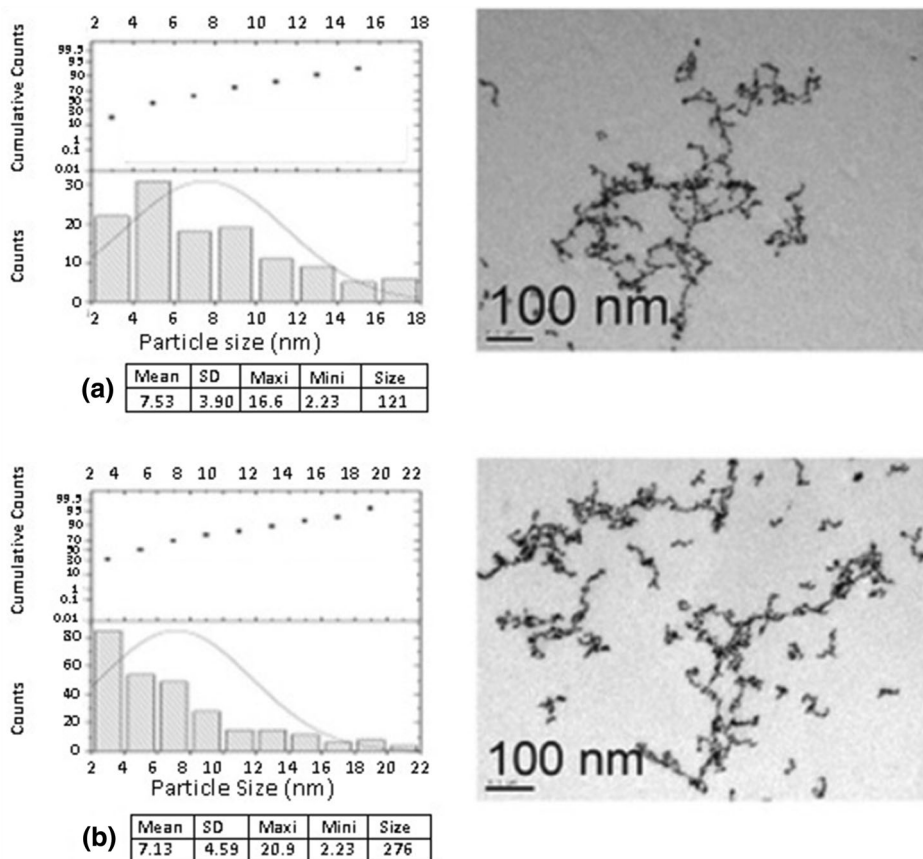
X-ray Diffraction

X-ray diffraction was applied only on nanoparticles samples supported on chitosan. Siemens diffractometer (model D-5000, German) with CuK radiation and Ni filter was utilized. The powder was identified by scanning at 2° 2θ/min of speed.

Results

In order to test the growth or aggregation of Au nanoparticles, the Au/2-propanol colloidal nanoparticles with a theoretical concentration were used, because it is almost

Fig. 1 Representative TEM micrographs of Au colloidal suspension after a drop casting on a carbon coated copper grid: **a** Nucleation time 0 h; **b** nucleation time 24 h



impossible to calculate the real concentration from the synthesis CLD or by the characterization techniques employed in this work. The theoretical concentration of Au nanoparticles in 2-propanol was 2.5×10^{-3} M. TEM micrographs (Fig. 1) show the morphology of the conglomerated colloidal of Au NPs. at 0, 6, 12 and 24 h. Au NPs. were assembled spontaneously in fractal agglomerates and their estimated average size was 6–7 nm, the nanoparticles were separated by the solvation sphere, 2-propanol solvated the Au atoms that were on the surface, nanoparticles shape was spherical.

Light scattering (LS) analysis showed a significant difference in the diameter of nanoparticles, in comparison to those observed in the TEM micrographs. LS measurements reported bigger sizes than those observed from transmission electron micrographs. This is due to LS perceives a sample as “a whole” and not as aggregated nanoparticles, not identifying size of each one separately.

Colloidal NPs were suspended as fractal aggregations, so LS does not discriminate between agglomerates or individual particles. In addition, LS is a dynamic measure, so, this type of analysis is usually correct for spherical particles, with some regularity in form and with a high degree of dispersion. Therefore, LS technique does not differ in form or can not specify whether the nanoparticle is

a cluster, an agglomeration or a single nanoparticle. It is clear, in this case and in the metal colloids measurements, there are agglomerated nanoparticles. This measure could only confirm that nanoparticles along time tended to aggregate and form big clusters (systems composed of many nanoparticles). Another factor in the LS measurement was the polydispersity, since it can determine nanoparticles shape. An increase in the polydispersity indicated that there were several shapes, such as when measuring irregular shapes of the fractals agglomerated. Also, it was possible to discriminate material shape, thus, a nanotube would indicate a wide size distribution, since the technique is essentially designed to spherical nanoparticles. The disadvantage of LS method is related to colloid size. A wide size distribution, produces a rapid blockage of filters, obtaining 1–2 μ L of colloid with uniform size. Measures of dynamic light scattering of gold nanoparticles at 0 h showed an effective diameter of 349.9 nm, and a polydispersity of 0.203 ± 9.3 nm. Thus, it could be appreciated for subsequent measures of Au nanoparticles at 6 and 24 h, that effective size obtained by light scattering increased until reach the effective diameter of 1486 nm and a polydispersity of 190 for Au nanoparticles at 24 h. This is because the size of the agglomeration increased its size after 0 h.

As shown in Fig. 1, every gold nanoparticle is closely linked to others and gaps can be distinguished between neighboring particles. The mechanism of nanoparticles formation involves the fractal aggregation because of solvent dipole–dipole interaction, and aggregation on the dispersions at substrate surface [8].

Either light scattering model for large spherical metal particles or by using the differential half-effective theory (Bruggeman's or Maxwell–Garnett's models) [9, 10] to small nanoparticles with different environmental refractive indices can be used.

There are many explanations suggested to justify some phenomenon of absorption [11, 12].

These include the quantum effects of size, wide distribution of particle sizes, for the absorption of particles resistant coating, the grouping of small metal particles and clusters, and formation of clusters and fractal aggregation. The resonant Plasmon caused a strong absorption in the optical range, and these values are investigated for non-linear optical applications [13, 14]. It is also indicative of the lifetime of the colloid, in this period the nanoparticles remain in suspension, showing a homogeneous solution in all its parts. The plasmon absorption of metal–metal is better explained as an association to post-synthetic activity of the colloid, where the energy of nanoparticle tends to even associate with each other, not forming a solid extended, but agglomeration of nanoparticles. The baseline not increased along time because the gold fractal agglomerate precipitate in 2-propanol after 1 week. The schematic procedure for the preparation of CS-Au composite is shown in Fig. 2. 2-propanol solvate the particles enabled the colloid to be soluble in the organic solvent and it was determined the size of gold nanoparticles during the synthesis by CLD and SMAD techniques. The polymer stabilized better Au NPs, because in the organic solvent, the nanoparticles were added until flocculation. Through the SMAD technique, the polymer avoids aggregation

because the nanoparticles incorporation was performed just in the co-deposition within the reactor.

FT-IR analysis was performed in the medium and far range in order to observe the interaction of nanoparticle core with the colloid shell and explain, in some sense, the relationship between support and colloid surface. Some authors reported interactions by CLD method [4], Fig. 3 shows the mid FT-IR spectra for Au coll. and free chitosan, which did not prove the strong interactions between nanoparticles and 2-propanol support. The far and mid spectra were not sufficient to prove the existence of a chemical interaction between solvent and nanoparticles. A broad peak at 3437 cm^{-1} was observed in the FT-IR spectra for CS and CS-Au. This band is attributed to the stretch vibration of $-\text{NH}_2$ and $-\text{OH}$ groups [15], for CS-Au NPs., this band shift at lower frequency, indicating that $-\text{NH}_2$ or $-\text{OH}$ were involved in the stabilization of NPs. The absorption bands at 1660 cm^{-1} were assigned to the acetamide group in low molecular weight CS and the absorption band at 1598 cm^{-1} was assigned to the “free” amine group [16]. An absorption band between 1620 and 1670 cm^{-1} was observed for chitosan, which varied according to the metal. The wavelength displacement of this band was due to the association of chitosan and metal [17].

According to the FT-IR spectra, the amine or the acetamide group of chitosan interacts with the metal. The band at 1420 cm^{-1} attributed to $-\text{OH}$ groups bending vibration disappeared in the CS-Au NPs, indicating that $-\text{OH}$ groups participates in the chelation [18]. Far IR spectra provided more evident information about the interaction of chitosan with nanoparticles. A band at far IR (179 cm^{-1}) appeared for CS-Au, which is attributed to the metal–metal interaction (M-M) of nanoparticles [19]. On the other hand, the band at 443 cm^{-1} was assigned to the M–N vibration. This band evidences the weak interaction between nanoparticles and chitosan matrix. There was a metallic particle duality,

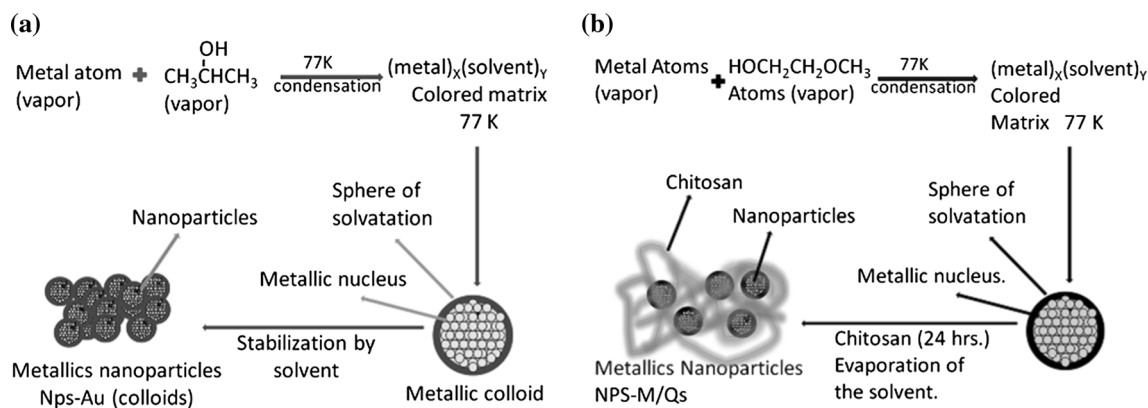


Fig. 2 Synthesis of Au colloids supported in chitosan: **a** CLD method; **b** SMAD method

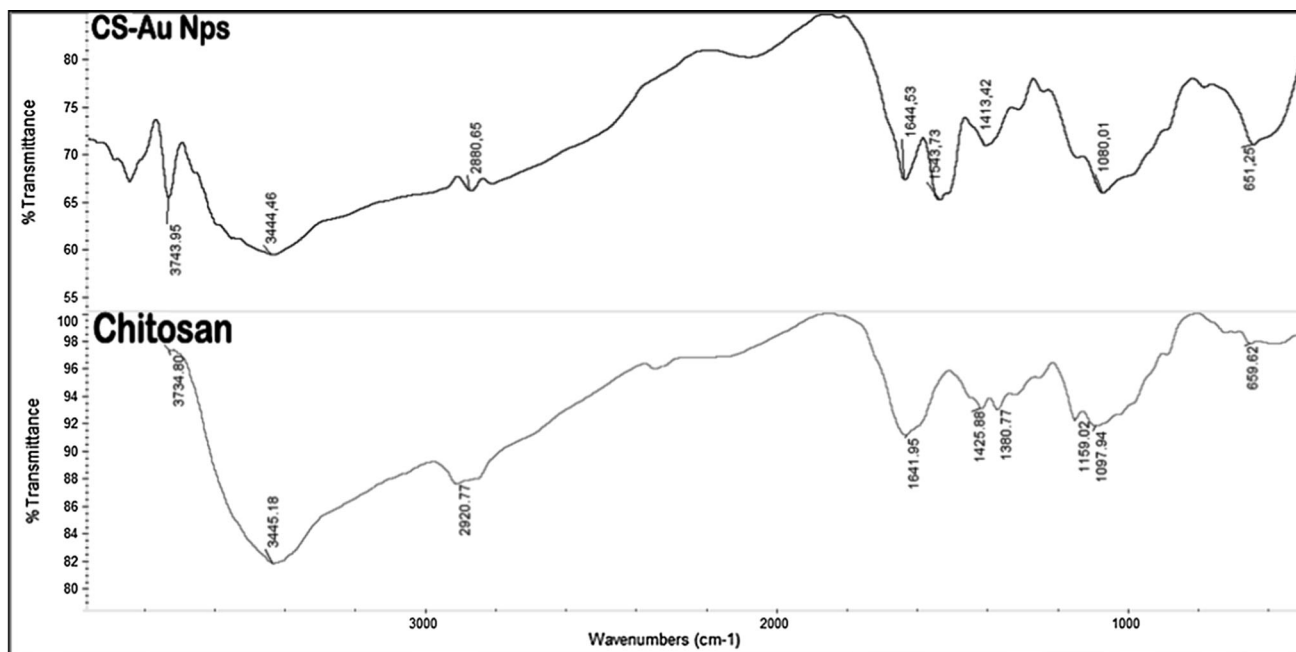


Fig. 3 Mid FT-IR spectra of: **a** CS-Au NPs; **b** Chitosan

presenting two forms, oxidized and not oxidized. This problem could be solved with the nanoparticles diffraction in order to identify the new diffraction ring corresponding to the oxidized compounds. Resin support and microtome cutting to obtain polymeric samples could increase the error and produce losses by diffusion of diffraction ring.

In addition, FT-IR spectra showed a new vibration which was not found in the compounds of “free” chitosan, attributed to the C=O stretch (amide II) due to the probable interaction with colloidal nanoparticles, with the amine group of the structure. It is also possible, according to what was reported by some authors [20, 21], the glycosidic rings of chitosan by the effect of chain hydrolysis reduces the molecular weight of chitosan; this hypothesis can be supported by the results obtained in the TGA. SMAD technique involves a stirring process where the metal atoms solvated can interact with the chitosan polymer chains [22].

Thermogravimetric analysis was determined for the metal NPs in chitosan. The measurements were conducted in order to observe how decreased the solvent boiling point with metal nanoparticles in it. This analysis confirmed that solvation of nanoparticles in the solvent, causing a decrease in the average rate of decomposition temperature. This was not observed for all samples because colloidal nanoparticles were in trace amounts.

Despite this, as shown in Fig. 4, at the end of temperature scan, at 313.4 °C, still remains at 0.25% by weight of the sample, which belongs to the metal nanoparticles.

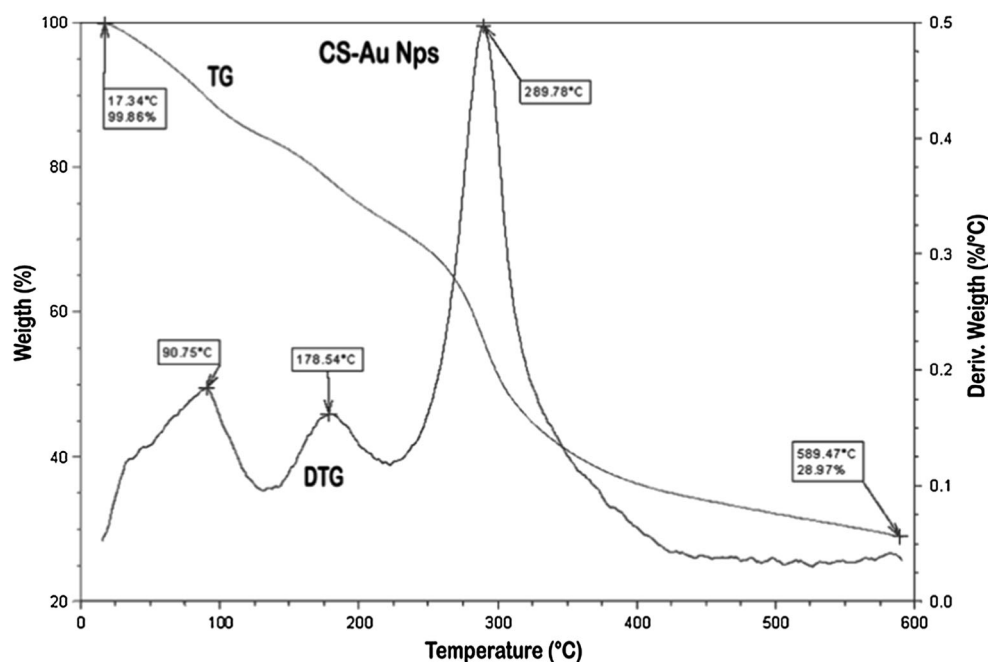
Figure 4 shows the thermogravimetric curves (TG) and its derivative (DTG) for chitosan with Au/2-propanol colloid.

Figure 4 shows the decomposition temperature of composite heated in a nitrogen atmosphere. The thermal degradation of CS and composites showed two weight loss stages, as shown in the literature [14]. The first weight loss took place at 96 °C due to the loss of adsorbed moisture and/or evaporation of the trapped water and residual 2-propanol. The second weight loss at 180 °C was more complex and includes the further degradation of glucosamine chains to yield the carbon and hydrocarbons.

The decrease in $T_d = 289$ °C (maximum weight loss rate) showed that composite may induce degradation of chitosan in the second step. Furthermore, T_d temperature for composite was lower than chitosan. Thermal stability of the composite was lower than pure chitosan, this reduced thermal stability was presumably as a result of the reduction in the number of intra and inter hydrogen bonds of chitosan after the trapping of Au nanoparticles. Additionally, they facilitate the removal of -OH and NH_2 groups that can interact with Au clusters.

When metallic Au was evaporated with the inclusion of gaseous alcohol, Au in oxidation state zero was complexed with the electron donating centers of the primary amine groups in chitosan, due to the strong coordinating interactions among them, back bonding type. When deposited metal atoms fall on the polymer surface, which grows simultaneously by polymer fragment deposition, the arriving metal atoms undergoes various processes such as a random distribution on the polymer surface, diffusion into the grown polymer, and desorption. The metal diffusion distance in such matrix is smaller than ordinary polymers, and metal atoms may encounter each other or be captured

Fig. 4 TGA, thermogram of CS-Au NPs



by matrix defects. This leads to strong aggregation and formation of stable metal nanoparticles in the polymer host. The colloids in the areas among several cavities agglomerate due to the van der Waals forces between solvated particles and the solvent confinement. Then at a compromised distance and perfect position giving the minimum free energy, ordering occurs in small domains along the boundary of the hole. The chitosan provided both the steric and electrostatic stabilization to the Au NPs. in the colloidal dispersion. As it is known, gold colloidal particles consist of an elemental gold core surrounded by a negative ionic double layer of charges, which prevent them from aggregation in solutions [19]. According to this, strong dipole–dipole interaction is believed to be the driving force of the nanoparticle self-organization. Previous research suggested that linear assembly of colloidal particles might take place in the presence of an intrinsic or induced dipole moment once the dipole–dipole interaction is strong enough to overcome the thermal energy and the electrostatic repulsion between the colloidal particles.

TEM analysis of chitosan doped with Au NPs showed their inclusion in the polymeric matrix, the problem also was the adsorption or absorption determination of nanoparticles in the matrix, as it was very difficult to make good electron diffractions, as shown in Fig. 5d. When it is possible, to have a good diffraction a new ring diffraction of metal oxidation would appear, this is not apparent because the nanoparticles are very small. Another phenomenon to be noted is the change of Au nanoparticles agglomeration shape, not adopting the fractal shape, but instead agglomerated in circular shape.

The composite prepared by solvated metal atom dispersed showed a morphology in which the metal Au NPs were uniformly dispersed in a polymer matrix (Fig. 5a). Dark field image of the composite is shown in Fig. 5c. The bright regions correspond to the highest atomic number of gold, and the dark one corresponds to the chitosan matrix. The TEM images demonstrate that Au nanoparticles aggregates in the polymer host and the spherical Au aggregates with sizes between 5 and 10 nm were not growing the polymer during depositions. Formation of metal nanoparticles in the polymer matrix can be described in the same way as cluster formation on the polymer surface.

It was not possible to refine completely the X-ray diffraction, as the polymer matrix doped with nanoparticles produces a diffraction which is a mixture of the diffraction of NPs and CS, showing no defined peaks and broad signals due to the structure semi-crystalline polymer or caused by very small crystal structures (nanocrystals) specially in case of metal nanoparticles [23]. In most cases, the diffractogram peaks overlap, preventing indexing of the diffraction peaks representative of the metal nanoparticle, it could only observe the peaks representing crystalline region of chitosan. Intermolecular hydrogen bonding caused that chitosan has a crystalline character and makes difference in most polymers composed of carbohydrates [18]. As shown in Fig. 6, the pattern of X-ray diffraction of chitosan showed high-intensity diffractions with the most characteristic points crystalline at 10.4° and 19.8°.

The pattern of X-ray diffraction of chitosan compounds doped with metal nanoparticles showed that characteristic peaks of chitosan were weakened and in some cases

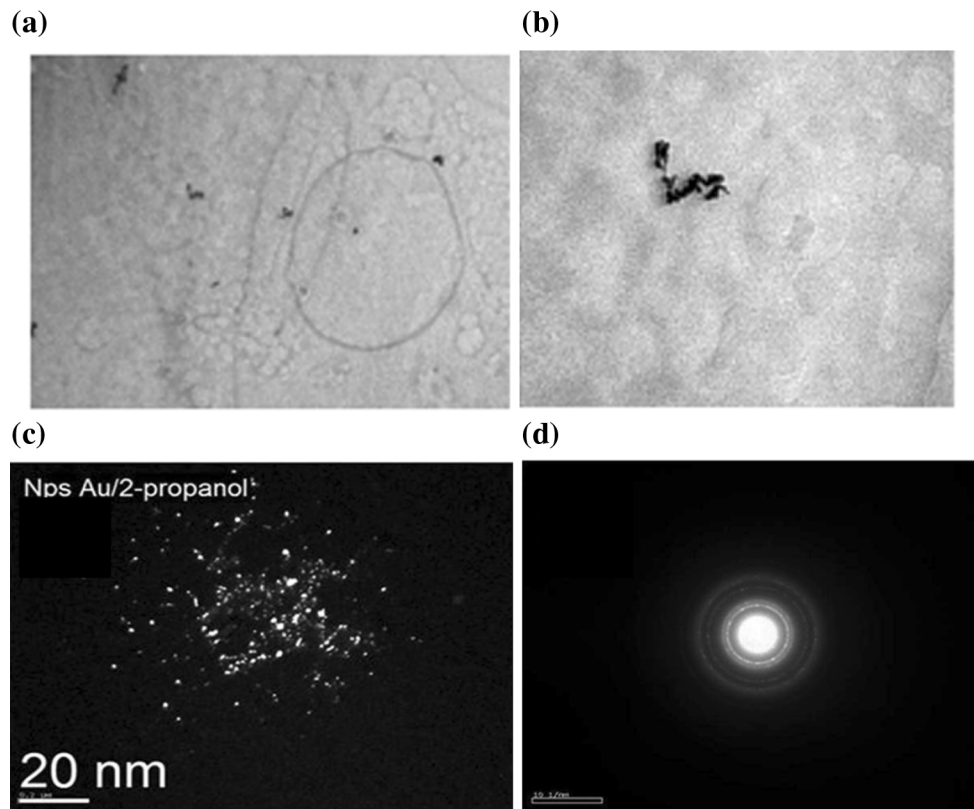


Fig. 5 TEM micrographs of Au nanoparticles supported in chitosan; **a** CS-Au NPs; **b** CS-Au NPs, obtained by SMAD technique, showing the nanoparticle agglomerates supported in chitosan; **c** dark field of

CS-Au NPs, showing the sphere nanoparticle and fractal aggregation; **d** diffraction pattern of Au NPs, supported in chitosan

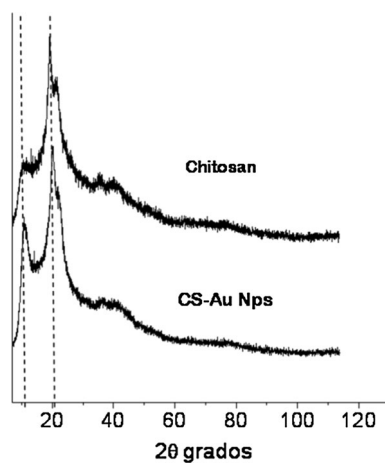


Fig. 6 X-ray powder diffractograms of CS and CS-Au NPs

disappeared, while new diffraction peaks appeared. This indicates the formation of a new regular crystalline phase [24], in which the diffraction peaks of chitosan disappeared because the hydrogen bond in the chitosan was destroyed by the metal nanoparticles, forming bonds with $-NH_2$ and $-OH$ groups. A low formation of hydrogen bonds, makes the chitosan chain breaking down and open, this causes that compounds have amorphous domains and allows a better

accessibility to the reagents, thus a better reactivity [18]. The distance to the crystallographic plane of chitosan was reported by using the Bragg's law [25].

Measures of field-emission scattering electron microscopy (FESEM) allowed images of high level (Fig. 7). With FESEM was possible to observe the surface and a few layers of 2–3 micrometers thick inside of the CS. It was not possible to accomplish an elemental analysis, but the image quality was much higher than the SEM technique. FESEM showed that nanoparticles were agglomerated in different forms, which imitate or resemble to disposition observed in colloids, this can be explained because SMAD method is a procedure similar to CLD method. SMAD respect to others methods, keeps the nanoparticles out of contact oxidizing atmospheres, so the metal found should have an oxidation state zero. Still, micrographs showed that metal was supported on the polymer surface and not included, as proposed the technique. This complicates metal analysis because the barrier should protect the polymer, however is not effectively enough to prevent metal oxidation (see Fig. 7) of FESEM micrographs of Au-CS composite.

The polymer stabilizes in a better way the gold nanoparticles in presence of organic solvent. Through the SMAD technique, the powder polymer prevents the

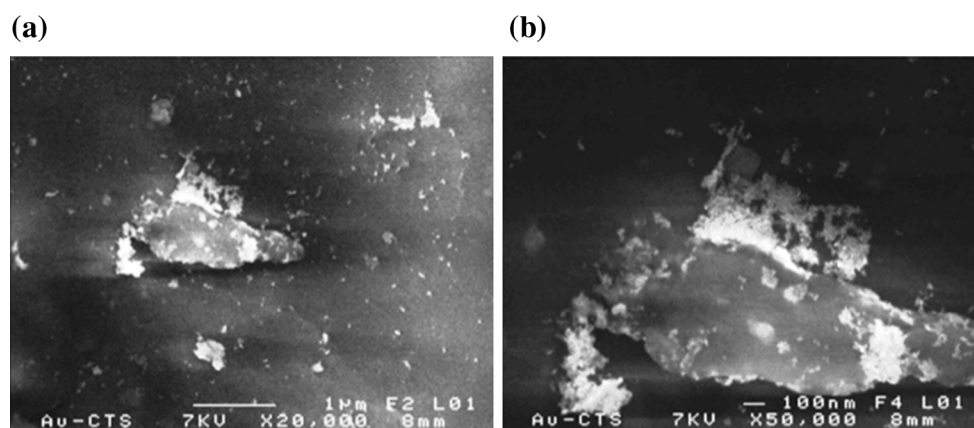


Fig. 7 FESEM micrographs of Au-Cs composite **a** close up $\times 20,000$, **b** close up $\times 50,000$

aggregation because the inclusion of nanoparticles was performed with the co-deposition during the reaction.

Conclusion

Au nanoparticles takes a fractal shape, these get agglomerated along the time. These agglomerations are typical Au suspensions, which were evidenced by the transmission electron micrographs taken in the study over time.

On the other hand, far FT-IR absorption of CS-Au NPs was associated to metal-metal gold clusters around 400 cm^{-1} [18].

The micrographs of dark-field transmission confirm the existence of nanoparticles in colloidal form. On the contrary, the FT-IR analysis for all samples colloidal not identify a chemical bond between metal/solvent but confirm metal/chitosan interaction.

Analysis performed by light scattering, contradict the conclusions drawn from TEM, where LS does not discriminate among nanoparticles shape, detected as a “whole” agglomerated in suspension.

The chitosan polymer matrix slows growing and aggregation of metal nanoparticles of gold by increasing its stability, but does not produce a good distribution before being stabilized in the polymer matrix. They are grouped in some way down the distribution of nanoparticles, which form agglomeration.

Acknowledgments This work was supported by FONDECYT 1080704 and 1140025. C. Cruzat-Contreras acknowledge Consejo Nacional de Ciencia y Tecnología de Chile (CONICYT) for scholarship grants.

Compliance with Ethical Standards

Conflict of interest The authors declare that they have no conflict of interest.

References

1. M. Pileni (2003). *Nat. Mater.* **2**, 145.
2. B. Khanra and M. Menon (2000). *Physica B* **291**, 368.
3. G. Cárdenas-Triviño, K. Klabunde, and B. Dale (1987). *Langmuir* **3**, 986.
4. M. Meléndrez, G. Cárdenas, J. Díaz, C. Cruzat, and J. Arbiol (2009). *Colloid Polym. Sci.* **287**, 13.
5. K. Oh, R. Kim, J. Lee, D. Kim, S. Cho, and S. Yuk (2008). *J. Appl. Polym. Sci.* **108**, 3239.
6. G. Cárdenas and J. Acuña (2001). *Colloid Polym. Sci.* **279**, 442.
7. M. Meléndrez, G. Cárdenas, J. Morales, J. Díaz, and C. Cruzat (2009). *Polym. Bull.* **62**, 355.
8. J. Liao, Y. Zhang, W. Yu, L. Xu, C. Ge, J. Liu, and N. Gu (2003). *Colloids Surf. A: Physicochem. Eng. Aspects* **223**, 177.
9. J. C. Kitchen and J. R. V. Zaneveld (1995). *Appl. Opt.* **34**, 31.
10. C. Pecharromán, A. Esteban-Cubillo, H. Fernández, L. Esteban-Tejeda, R. Pina-Zapardiel, J. Moya, J. Solis, and C. Afonso (2009). *Plasmonics* **4**, 261.
11. P. Sen and D. Tanner (1982). *Phys. Rev.* **B 26**, 3582.
12. R. Ruppin (1979). *Phys. Rev.* **B 19**, 1318.
13. S. Forster (2003). *Top. Curr. Chem.* **226**, 1.
14. Z. Chen, C. Zhang, Y. Tan, T. Zhou, H. Ma, C. Wan, Y. Lin, and K. Li (2015). *MicrochimActa* **182**, 611.
15. G. Cárdenas, J. Díaz, M. Meléndrez, C. Cruzat, and A. García (2009). *Polym. Bull.* **62**, 511.
16. L. Tang and D. Hon (2001). *J. Appl. Polym. Sci.* **79**, 1476.
17. S. Brewer, S. Anthireya, S. Lappi, D. Drapcho, and S. Franzen (2002). *Langmuir* **18**, 4460.
18. X. Wang, Y. Du, L. Fan, H. Liu, and Y. Hu (2005). *Polym. Bull.* **55**, 105.
19. J. Alvino, T. Bennett, D. Anderson, B. Donoeva, D. Ovoshchnikov, R. Adnan, D. Appadoo, V. Golovko, G. Andersson, and G. Metha (2013). *RSC Adv.* **3**, 22140.
20. C. Sun, R. Qu, H. Chen, C. Ji, C. Wang, Y. Sun, and B. Wang (2008). *Carbohydr. Res.* **343**, 2595.
21. C. Mayer, S. Neveu, C. Simonnet-Jégat, C. Debiehime-Chouvy, V. Cabuil, and F. Secheresse (2003). *J. Mater. Chem.* **13**, 338.
22. G. Cárdenas and P. Shevlin (1984). *J. Org. Chem.* **49**, 4726.
23. D. Cockayne (2007). *Annu. Rev. Mater. Res.* **37**, 159.
24. R. Muzzareli and A. Ferrero (1972). *Talanta* **19**, 1222.
25. G. Clark and A. Smith (1936). *J. Phys. Chem.* **40**, 863.